How pristine is the interior of the comet 67P/Churyumov–Gerasimenko?

Maria Teresa Capria, Fabrizio Capaccioni, Gianrico Filacchione, Federico Tosi, Maria Cristina de Sanctis, Stefano Mottola, Mauro Ciarniello, Michelangelo Formisano, Andrea Longobardo, Alessandra Migliorini, et al.

Monthly Notices
of the
ROYAL ASTRONOMICAL SOCIETY

MNRAS **469,** S685–S694 (2017) doi:10.1093/mnras/stx2627

How pristine is the interior of the comet 67P/Churyumov–Gerasimenko?

Maria Teresa Capria,[1⋆] Fabrizio Capaccioni,[1⋆] Gianrico Filacchione,[1⋆] Federico Tosi,[1] Maria Cristina De Sanctis,[1] Stefano Mottola,[2] Mauro Ciarniello,[1] Michelangelo Formisano,[1] Andrea Longobardo,[1] Alessandra Migliorini,[1] Ernesto Palomba,[1] Andrea Raponi,[1] Ekkehard Kührt,[2] Dominique Bockelée-Morvan,[3] Stéphane Erard,[3] Cedric Leyrat[3] and Angelo Zinzi[4]

[1]*Istituto di Astrofisica e Planetologia Spaziali (IAPS), INAF, via del Fosso del Cavaliere, I-00133 Roma, Italy*
[2]*German Aerospace Center (DLR), Institute of Planetary Research, Rutherfordstrasse 2, D-12489 Berlin, Germany*
[3]*LESIA, Observatoire de Paris, LESIA/CNRS, UPMC, Université Paris-Diderot, F-92195 Meudon, France*
[4]*ASI Space Science Data Center (SSDC), Agenzia Spaziale Italiana, via del Politecnico, I-00133 Roma, Italy*

Accepted 2017 October 6. Received 2017 October 4; in original form 2017 March 23

ABSTRACT

Comets are usually considered to be the most primitive bodies in the Solar System. The level of truth of this paradigm, however, is a matter of debate, especially if by primitive we mean that they represent a sample of intact, unprocessed material. We now have the possibility of analysing the comet 67P/Churyumov–Gerasimenko with an unprecedented level of detail, but its interior remains largely unprobed and unknown. The questions we address in this paper concern the depth of the processed layers, and whether the comet nucleus, under these processed layers, is really representative of the original material. We applied the Rome model for the thermal evolution and differentiation of nuclei to give an estimation of the evolution and depth of the active layers and of the interplay between the erosion process and the penetration of the heat wave. In order to characterize the illumination regime and the activity on the nucleus, two locations with very different illumination histories were chosen for the simulation. For both locations, the bulk of the activity tends to be concentrated around the perihelion time, giving rise to a high erosion rate. As a consequence, the active layers tend to remain close to the surface, and the interior of the comet, below a layer of few tens of centimetres, can be considered as pristine.

Key words: comets: general – comets: individual: 67P/Churyumov–Gerasimenko.

1 INTRODUCTION

Comets are usually considered to be the most primitive bodies in the Solar System, remnants and specimens of the objects that accreted in the external regions of the protosolar disc (Mumma & Charnley 2011). The level of truth of this paradigm, however, is a matter of debate. If primitive denotes that the comets not only are remnants of the formation process, but also that they represent a sample of intact, unprocessed material, this is a completely different claim. Considering the long dynamical evolution of a comet, during which the chaotic orbit could have brought the body closer to the Sun than it is at present, and a possible collisional evolution, it is not obvious that the material constituting the nucleus really is pristine, at least in the interior. Together with non-disruptive evolutionary processes, some special properties of the cometary material are required in order to minimize the effects of the interaction with the environment. The most important one is that the material must be almost impenetrable to thermal waves, which means it must be very insulating, in order to prevent devolatilization, chemical alteration and physical processes that in general would change not only the composition but also the original physical properties.

Comets are active, however, so at least the layers close to the surface are surely processed by heat waves and interaction with the external environment. The questions we are trying to address in this paper concern the depth of the processed layers, and whether the comet nucleus, under these processed layers, is really representative of the composition and physical properties of the original material.

We now have the opportunity to analyse the comet 67P/Churyumov–Gerasimenko (67P) with an unprecedented level of detail. Comet 67P has been extensively observed not only from ground-based telescopes but also remotely and in situ by the instruments onboard the ESA mission *Rosetta* (Schulz 2012).

⋆ E-mail: mariateresa.capria@iaps.inaf.it (MTC); fabrizio.capaccioni@iaps.inaf.it (FC); gianrico.filacchione@iaps.inaf.it (GF)

Rosetta, after its launch in 2004, arrived at the comet in 2014 August and orbited the comet until 2016 September. *Rosetta* carried a comprehensive suite of instruments that observed the nucleus and the coma at the same time during the inner part of the orbit of 67P around the Sun and collected various kinds of data. It also deployed the lander *Philae* in 2014 November; notwithstanding its short life, the lander was able to provide valuable data.

All the instruments carried by *Rosetta* and *Philae* probed only the surface and the coma of 67P. The only exception is the radar CONSERT (Kofman et al. 2007), which by sensing the dielectric properties of the interior can infer some structural properties of the nucleus. This means that most questions about the macrostructure and the physical characteristics (composition, temperature, ice state) of the internal layers and about the thickness of active/processed layers will not have a direct answer.

The preceding questions are related directly to the most important question: how pristine (i.e. unprocessed) is the nucleus under the surface layers? This information can give fundamental clues and constraints on the formation process of the comet and on its dynamical and evolutionary history. It is also extremely relevant for any future comet sample return mission that would bring back samples as representative as possible of the original, primordial material.

The erosion of the surface has been modelled by Keller et al. (2015), who investigated the illumination of the surface to predict the water sublimation. These authors concluded that the average erosion at each orbit, directly computed from the water sublimation, can be from 0.7 to 3 m, depending on the model.

Even though the instruments onboard *Rosetta* and *Philae* did not directly probe the interior of the nucleus, they provided many clues as to its structure and status, clues that can be used to infer the condition of the interior and constrain in an unprecedented way thermal models giving information on the depth of active layers and the status of the interior in general. In this paper, the results of a thermal evolution and differentiation model of the nucleus, applied to 67P to study the thickness of processed layers, are presented and discussed. The paper is organized as follows: in Section 2 the observations of *Rosetta* relevant to the interior are reviewed; in Section 3 the model is described; in Sections 4 and 5 the results are described; and the discussion and conclusions can be found in Sections 6 and 7.

2 INFORMATION FROM ROSETTA

Rosetta carried a complete set of instruments, which enabled a thorough investigation of the nucleus surface and the coma of comet 67P. The spacecraft orbited the comet for 2 yr, and a good number of papers have already been published with the first analyses and interpretation of the observations. Information related to the subject of the paper is briefly reviewed in the following.

The comet 67P has an orbital period of 6.44 yr, and aphelion and perihelion are located, respectively, at 5.683 and 1.243 au. The rotation period of the comet has been observed to change at each perihelion passage during the past three apparitions. Mottola et al. (2014) reported values of 12.76129 and 12.4043 h for the period before and after the 2009 perihelion passage, respectively, while the current, post-2015 perihelion rotation period is about 12.0 h.

The nucleus has a complex, highly irregular bilobate shape (Sierks et al. 2015). The obliquity of the spin axis is large (52°); as a consequence, the nucleus undergoes strong seasonal effects, causing extreme variations in solar irradiation and activity. This complex geometry causes a pronounced difference between the two hemispheres: while the southern hemisphere receives a large amount of solar energy during a short time centered around the perihelion, the northern hemisphere receives a lower amount but over a much longer timespan.

Information on the interior comes primarily from gravity field measurements and the radar CONSERT.

The mass and gravity field, derived from measured spacecraft velocity perturbations, enable the mass, bulk density, porosity and internal structure of the nucleus to be inferred (Pätzold et al. 2016; Jorda et al. 2016). The average bulk density of the nucleus was found to be 533 ± 6 kg m^{-3}. The interior appears to be homogeneous and with constant density at a global scale. A high porosity, namely greater than 0.7, is implied.

From the propagation time and form of the signals, it was determined from the radar experiment CONSERT that the upper part of the 'head' of 67P is fairly homogeneous on a scale of tens of metres (Kofman et al. 2015).

The thermal properties of the surface and of the layers under the surface have been measured by the imaging spectrometer VIRTIS (Coradini et al. 2007), the microwave instrument MIRO (Gulkis et al. 2007), and MUPUS, the sensors package on *Philae* (Spohn et al. 2007). VIRTIS, which is sensitive to diurnal surface temperatures > 170 K with accuracy increasing with increasing temperature, derived temperatures typical of dusty, low-thermal-inertia surfaces (Tosi et al. 2015). The local thermal conductivity has been determined by MUPUS at the *Philae* landing site to be very low, of the order of 10^{-3} W K^{-1} m^{-2} (Spohn et al. 2015). MIRO probed temperatures in the shallow subsurface (Gulkis et al. 2015; Schloerb et al. 2015; Choukroun et al. 2015); the emission arises from depths between approximately 1 and 4 cm below the surface, depending on the channel. MIRO observations are consistent with a low thermal inertia in the range $I = 10$–30 J K^{-1} m^2 s$^{-0.5}$ and a thermal skin depth of approximately 1 cm.

The dust/ice ratio in the nucleus can be estimated from the data on the gas and dust in the coma, besides those on porosity and bulk density. A first estimation (from 4 to 10 times more dust than ice by mass) has been obtained through a gravity experiment (Pätzold et al. 2016) and was confirmed by the GIADA experiment (Colangeli et al. 2007; Rotundi et al. 2015).

The presence (or absence) of high-volatility ices gives important clues on the status and temperature of the interior.

High-volatility ices have been detected by the mass spectrometer ROSINA (Balsinger et al. 2007; Le Roy et al. 2015; Fuselier et al. 2015) and MIRO (Rubin et al. 2015; Lee et al. 2015). This implies that the internal temperature cannot be higher than 100 K, if these species are trapped as gas in amorphous water ice; if instead they are present in their ice form the temperature could be as low as 30 K (Collings et al. 2004).

Clues on the depth of sublimation fronts and on the thickness of active layers come from observations on the activity, in particular those correlating locally the gas and dust activity with the illumination conditions (the thickness of the layer can be deduced from the lag between illumination and the onset of the activity). From the data collected by VIRTIS (Filacchione et al. 2016; De Sanctis et al. 2015) and ROSINA (Mall et al. 2016) it can be deduced that the active layers are not far from the surface.

H_2O ice patches were also observed in the OSIRIS data (Keller et al. 2007; Pommerol et al. 2015; Barucci et al. 2016; Raponi et al. 2016; Fornasier et al. 2016), with an extent of few metres. These exposed water regions show changes in the appearance over a timespan of 2 weeks, which might be attributable to differences in the illumination conditions.

Another relevant piece of information comes from the erosion of the surface estimated from the images of OSIRIS. This can help in determining how pristine the surface being exposed is (an interplay between the erosion and the penetration of the heat wave). It has been estimated that a layer of 1.0 ± 0.5 m is lost during each comet passage in the inner Solar System (Bertaux et al. 2015). OSIRIS did observe erosion and collapsing phenomena, together with many other morphological changes (Keller et al. 2015; Auger et al. 2015; Lucchetti et al. 2016; Thomas et al. 2015; Vincent et al. 2015).

3 NUCLEUS THERMAL MODELLING: THE ROME MODEL IN THE *ROSETTA* ERA

Thermal and differentiation models of the nucleus are useful because they can be used not only to test hypotheses on the physical processes acting in the nuclei but also to infer activity and interior properties over the whole orbital period. The results of these models depend heavily on many parameters describing the cometary matter and its properties. For the first time, most of these parameters have now been constrained or even determined by *Rosetta*. This fact and the amount of information yet to be fully interpreted are forcing modellers to update the way in which matter and physical processes are described and schematized in thermal models of the nucleus.

The 'Rome model' has been developed and used in different versions (Capria et al. 2009, 2012; De Sanctis, Lasue & Capria 2010; De Sanctis et al. 2010). Below we briefly summarize its latest version.

Following recent publications, comets can form by gravitational collapse of centimetre-sized dust agglomerates in the early Solar System (Johansen et al. 2007; Skorov & Blum 2012; Blum et al. 2014; Pfalzner et al. 2015), giving birth to cometesimals composed of dust and ice micrometre-sized particle aggregates. In the model, the comet matter is described as a porous mixture of dust-grain aggregates and ices. Ices are composed of water and up to two different species, typically CO and CO_2 that, after H_2O, are the major constituents of the volatile part of the nucleus (Bockelée-Morvan et al. 2004). Water ice can be initially amorphous, and in this case a fraction of the more volatile gases can be trapped in the amorphous matrix and released during the transition to the crystalline phase and the sublimation of water ice (Bar-Nun and Laufer 2013, and references therein).

The refractory component is represented as up to two size distributions of grain aggregates characterized by a density and a specific heat. The thermal conductivity of the aggregates is computed following the expression given in Gundlach & Blum (2012). The expression takes into account both the heat conduction through the solid material and the heat transport owing to radiation within the pores of the material, and depends on the radius of the aggregates.

Energy and mass conservation are expressed by a system of coupled differential equations. Energy conservation is expressed as

$$\rho c \frac{\partial T}{\partial t} = \nabla(\mathrm{K} \cdot \nabla T) + Q_{\mathrm{H2O}} + Q_{\mathrm{CO2}} + Q_{\mathrm{tr}}, \quad (1)$$

where ρ, c and K are the bulk density, specific heat and thermal conductivity, Q_{H2O} and Q_{CO2} are the energy exchanged by the solid matrix in the sublimation and recondensation of the ices, and Q_{tr} accounts for the energy released during the phase transition from amorphous to crystalline ice. The model is one-dimensional and applied to a shape model under the assumption that lateral heat transport can be neglected, so the equation becomes (in spherical coordinates):

$$\rho c \frac{\partial T}{\partial t} = K \left[\frac{2}{r} \frac{\partial T}{\partial r} + \frac{\partial^2 T}{\partial r^2} \right] + \frac{\partial K}{\partial r} \frac{\partial T}{\partial r} + Q_{H2O} + Q_{CO2} + Q_{tr}. \quad (2)$$

Mass conservation is expressed as

$$\frac{\partial \rho}{\partial t} = -\nabla \Phi + Q*, \quad (3)$$

where ρ is the gas density, Φ is the flux and $Q*$ is the gas source term due to sublimation and recondensation processes.

Gas diffusion coefficients are computed on the basis of the mean free path of the molecules in the pore system, and the model accounts for three different diffusion regimes: Knudsen, viscous and transition.

The temperature on the surface is obtained by a balance between the solar input and the energy re-emitted in the infrared, conducted in the interior and used to sublimate ices if they are present on the surface.

The surface boundary condition used to solve the diffusion equation when ice is present on the surface is $P = P_{\mathrm{sat}}(T)$, where P is the gas pressure and P_{sat} is the saturation pressure. When no ice is present, the surface boundary condition is obtained assuming free sublimation at the comet nucleus surface: $P = 0$.

When the temperature rises, ices start to sublimate, beginning from the more volatile species; even if the nucleus is initially homogeneous a differentiated, layered structure is always obtained, in which the boundary between the different layers is a sublimation front.

Surface erosion resulting from ice sublimation and particle ejection is simulated in the model.

Particles on the surface can be blown off to become part of the dust flux; they are moving under the opposing effects of gravity and gas flux. To determine how many particles can be blown off to contribute to the dust flux, the various forces acting on a single aggregate are compared. In this way it is possible to obtain for each distribution a size range representing the radii of the aggregates that can leave the surface of the comet.

The illumination conditions at any given time and date around the orbit are provided by SPICE-based routines (Acton 1996).

3.1 Application of the model

A thermal model depends not only on the assumptions of the model itself, but also on the values attributed to its initial parameters. These parameters describe the initial state of the body and the properties of the matter of which it is composed. Most of them are now defined, derived or constrained from *Rosetta* observations. A given set of these parameters defines a 'Case'. By changing some of these parameters, and keeping all the rest fixed, different Cases can be built that are the subject of the simulation.

The parameters that have been used in the simulations described in this work are as far as possible obtained from the results of the *Rosetta* mission; some of them are collected in Table 1. The bulk density of the nucleus is assumed to be 470 kg m^{-3} because the latest, more accurate value was not available at the time the simulations were carried out; the average thermal conductivity is very low, of the order of 10^{-3} W K m, and the corresponding thermal inertia is in the range 12–25 J K^{-1} m^2 $s^{-0.5}$.

Two Cases, with different initial values for the ice/dust ratios, have been defined. In Case 1, the dust/ice ratio is 4, while in Case 2 it is 10. Parameters not constrained by *Rosetta* observations and

Table 1. Parameters describing the initial conditions of the nucleus for the two Cases studied in this work.

	Case 1	Case 2
Dust/ice ratio (in mass)	4	10
CO_2/H_2O	0.03	0.03
Dust distribution size range [m]	10^{-6} – 10^{-2}	10^{-6} – 10^{-2}
Dust density [kg m^{-3}]	10^3	10^3
Initial uniform temperature [K]	50	50

used to describe the initial conditions of the nucleus are the amount of minor ice species with respect to water contained in the nucleus, the state of the water ice itself, and the size distribution of dust grains in the nucleus. Here it is assumed that water ice is initially amorphous, and that a certain amount of the more volatile species is trapped and released during the transition to crystalline ice. An initial temperature compatible with the existence of amorphous ice has been chosen, 50 K. The percentage of CO_2 with respect to water initially present in the nucleus is 0.03.

A set of parameters describes the refractory component. The refractory component is simulated by a distribution whose properties are based on GIADA and OSIRIS measurements (Rotundi et al. 2015; Fulle et al. 2015, 2016). The refractory component in the coma is dominated by compact aggregates, with an average density of $\sim 10^3$ kg/m^3 and sizes ranging from 10^{-6} to 10^{-2} m and following a Gaussian distribution (Table 1).

From the results of VIRTIS and OSIRIS (Capaccioni et al. 2015; Sierks et al. 2015; Pommerol et al. 2015), the surface is dark, depleted in volatiles, and organics-rich. The maximum percentage of surficial water ice is about 5 per cent in the recently exposed, collapsed structures observed by VIRTIS (Filacchione et al. 2015), while higher values, up to 14 per cent, are measured on the active areas in Hapi region, where the condensation of the ice is associated with the diurnal illumination cycle (De Sanctis et al. 2015).

The comet 67P has been on its current orbit for a relatively short time, namely since 1959, when it had a close encounter with Jupiter that modified the orbital parameters (Maquet 2015). The semimajor axis was reduced from about 4.3 to 3.5 au, and the perihelion distance was reduced from about 2.7 to 1.3 au. Before 1959, the comet was orbiting far from the Sun.

At the beginning of the computations the nucleus is homogeneous in temperature and composition, and the water ice is assumed to be in the amorphous state. We start our simulations from the Kuiper belt (semimajor axis = 50 au, eccentricity = 0.5) with a simplified spherical shape, following the so-called multistage injection process (De Sanctis et al. 2006) of the nucleus to the internal Solar System (first an orbit with semimajor axis = 25 au and eccentricity = 0.4, then an orbit with semi-major axis = 8 au and eccentricity = 0.5). After that, we used the current orbit and the actual shape. The model follows the evolution during the multistage orbits and the beginning of the current orbit with a coarser timestep for a time long enough to stabilize the results, and then a much shorter timestep, of the order of seconds, is used to obtain results in the time intervals that are the object of the simulation (from 2014 onwards). After this long stabilization process, internal temperatures are no longer uniform in the layers close to the surface, and minor species sublimation fronts and a water ice crystallization front appear according to their volatility level, the deepest being the crystallization front, followed by the CO_2 sublimation front. When the nucleus begins to run on its current orbit, low-volatility ices and amorphous ice are still close to the surface, owing to the extremely low level of activity permitted by the past orbits.

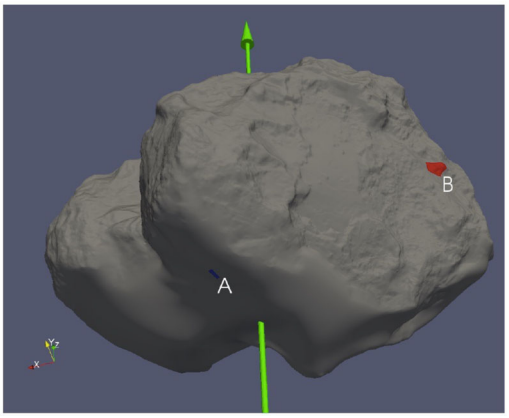

Figure 1. Positions of the two locations A and B on the surface of the comet.

The simulations are run on a given location defined by latitude and longitude on the digital shape model SHAP5 (Jorda et al. 2016). The computations are extremely time-consuming and require powerful processing resources. Running the code for the whole shape model representing the nucleus would require a computation power well above what is now available to the authors, and moreover it is beyond the scope of this work. One practical solution is to run the code only on selected locations, considered as representative of larger areas. The computations are actually performed on a grid of five points centered around each chosen location, to ensure that the averaged results are representative of the chosen area and not of a single topographic feature.

4 RESULTS OF THE SIMULATION: TWO DIFFERENT ILLUMINATION HISTORIES

This aim of this work is to give an estimation of the evolution and depth of active layers and of the interplay between the erosion process and the penetration of the heat wave. In order to characterize the illumination regime and the activity on the nucleus, two locations with different illumination histories have been chosen for the simulation; the two locations can be considered as representative of the different illumination regimes that can be experienced by the nucleus.

The chosen locations, shown in Fig. 1, are on the 'body' of the comet, in the Anhur region at a latitude of 55°S and a longitude of 69°E (A), and at the border between the Imhotep and the Ash regions at a latitude of 10°N and a longitude of 180°E (B). In order to characterize the activity in the two locations, the results will be described for the epochs of low and high activity.

4.1 A few days in the life of a comet – location A

The first location was chosen in the Anhur region, in an area characterized by the presence of boulders and various kinds of deposits (Lee et al. 2016). In this area *Rosetta*/VIRTIS detected the presence of CO_2 ice (2015 March) for a short period of time, with the ice being completely sublimated after a few weeks (Filacchione et al. 2016). In the same region, in 2015 May, OSIRIS identified large (1500 m^2) water-ice-rich patches that appeared and then vanished in about 10 d (Fornasier et al. 2016).

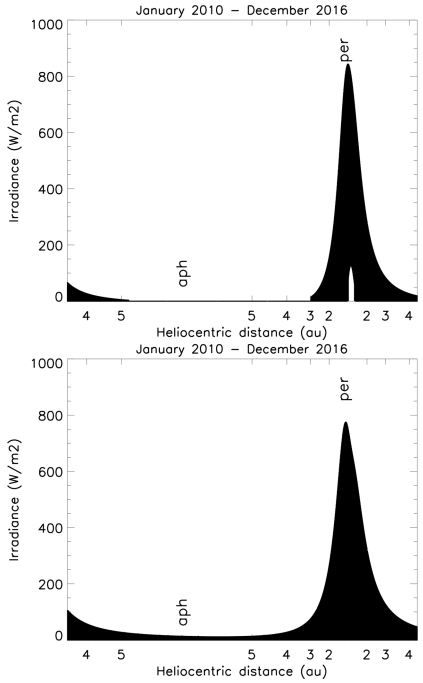

Figure 2. Solar irradiance with respect to the heliocentric distance at locations A (upper panel) and B (lower panel) in the time range 2010–2016.

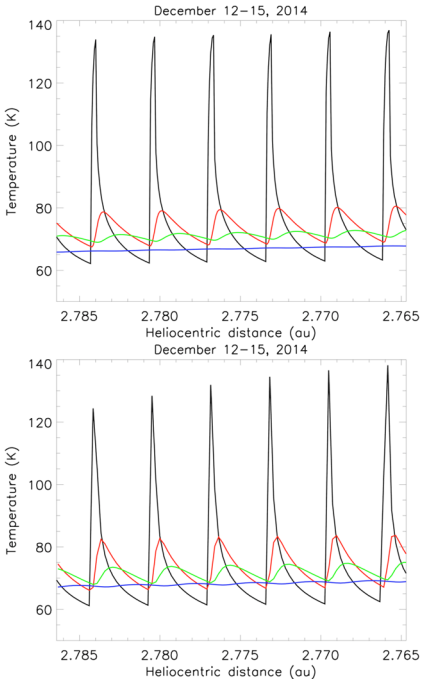

Figure 3. To illustrate the activity typical of this area, plots for both Cases are shown referring first to a period of low activity (2014 December, heliocentric distance = 2.8 au) and then to a period of high activity, centred around the perihelion time (2015 August 12, heliocentric distance = 1.243 au).

The illumination history of location A can be seen in Fig. 2 (upper panel). Owing to the large obliquity of the spin axis, the area is characterized by a long time, half of the orbital period (from 2011 March to 2014 November), without solar illumination. Then, after 2014 November, at a heliocentric distance of 2.98 au pre-perihelion, an increasing amount of solar energy reaches the surface. Around perihelion (2015 August 12) the region experiences a brief but extremely intense period of illumination, culminating in a month and a half during which the location is constantly illuminated.

In 2014 December, after years of darkness, point A is illuminated for 50 min per cometary day (12.4 h) at a very large minimum solar incidence angle (80°). The surface temperature reaches a maximum of 140 K for Case 1 (Fig. 3, upper panel, black line) and decreases down to 80 K at 2.5 cm below the surface (red line); 10 cm under the surface (blue line) the temperature has an almost constant value of 65 K. The activity is modest, and the gas flux consists mainly of CO_2. The sublimation front of the CO_2 ice and the transition front of the amorphous ice remain at a constant depth of 5 cm.

Surface temperatures, and, to a lesser extent, internal temperatures, are considerably higher for Case 2 (Fig. 3, bottom panel). As for the interior, in Case 2 thermal conductivity is slightly higher, owing to the higher percentage of refractory material. The gas flux and dust flux are even lower than in Case 1.

Around perihelion, the situation is completely different. During this period the area experiences, from August 12 onwards, a few weeks of constant illumination. Surface temperatures are much higher (Fig. 4), and drop off by as much as 50 K at 2.5 cm below the surface for both Cases. Owing to the slightly higher thermal conductivity, the heat wave penetrates to a greater depth in Case 2. As in the period of low activity, 10 cm under the surface the temperature, which is slowly rising, can be considered almost constant during the cometary day. During the period of constant illumination there is a dramatic change in the minimum surface temperatures, now around 200 K. The gas and dust fluxes (Figs 5 and 6) are very

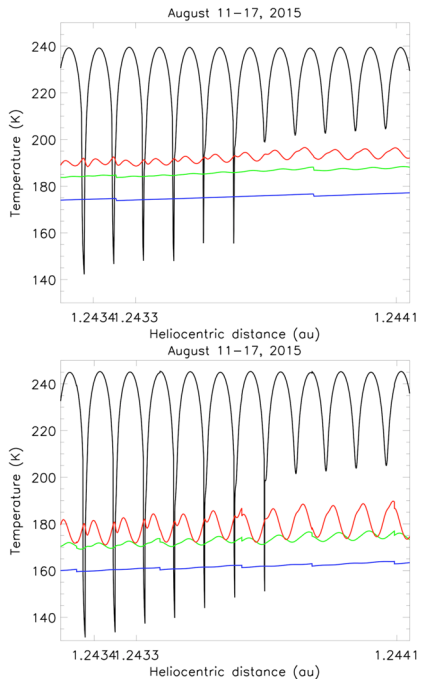

Figure 4. Case 1 (upper panel) and Case 2 (lower panel), location A, 2015 August 11–17: temperatures are given on the surface (black line) and in the layers below the surface (red line, 2.5 cm; green line, 5 cm; blue line, 10 cm).

strong. For Case 1, the water flux is about 0.5×10^{28} molec s^{-1} m^{-2} and the dust flux is of the order of 10^3 kg s^{-1}. For Case 2, the water flux reaches 10^{28} molec s^{-1} m^{-2} and the dust flux is of the order of 10^3 kg s^{-1}. The CO_2 flux, in both Cases, is almost constant during

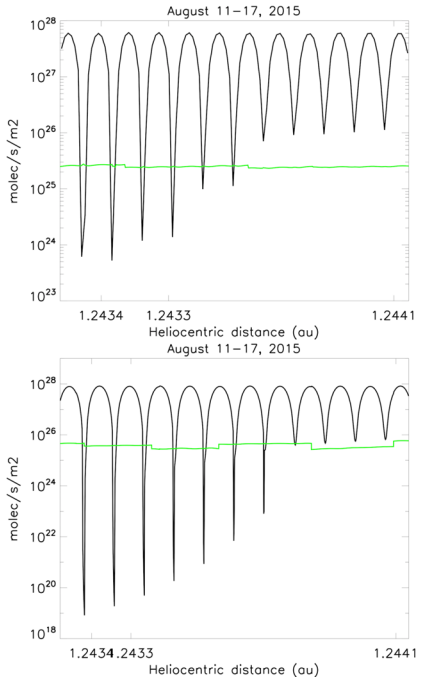

Figure 5. Case 1 (upper panel) and Case 2 (lower panel), location A, 2015 August 11–17: water flux (black line) and CO_2 flux (green line

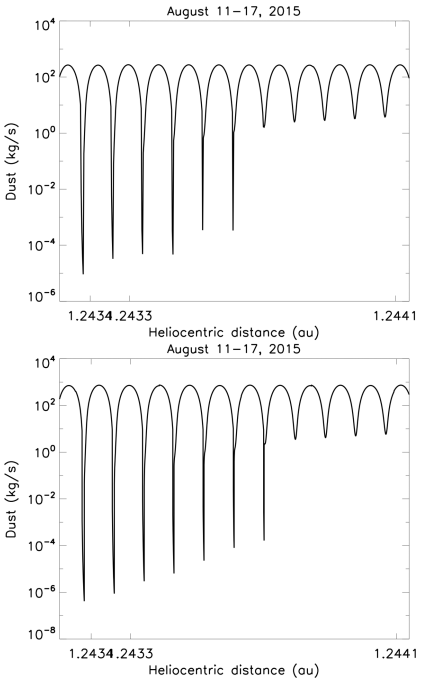

Figure 6. Case 1 (upper panel) and Case 2 (lower panel), location A, 2015 August 11–17: dust flux.

the cometary day, because it is coming from a layer 20 cm below the surface (Fig. 7).

The regime changes when, immediately after the perihelion, the location is constantly illuminated: the maximum values of all the fluxes do not change, while the minimum values strongly increase.

The corresponding stratigraphy during the year 2015 for both Cases is shown in Fig. 7. For Case 1, the CO_2 sublimation front that was initially a few centimetres under the surface is, at 2 au

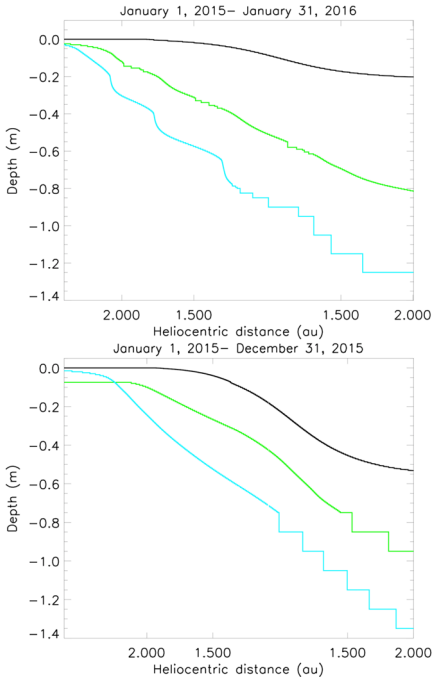

Figura 7. Case 1 (upper panel) and Case 2 (lower panel), location A, 2015 January 1 – 2016 January 31: stratigraphy showing the surface (black line), the CO_2 sublimation front (green line) and the amorphous ice transition front (blue line).

post-perihelion, 60 cm below the surface; in the same period the amorphous–crystalline transition front sinks by 1.15 m. The surface is eroded, in 1 yr, by 20 cm. For Case 2, the CO_2 sublimation front, initially 7 cm under the surface, is at 40 cm when the comet is at 2 au post-perihelion. The amorphous ice transition front, which was 2 cm under the surface, is by the end of the year 80 cm below the surface. In Case 2 the surface is eroded by 55 cm.

4.2 A few days in the life of a comet – location B

Location B lies on the body of the comet, in the Imhotep region, close to the border with the Ash region, at a latitude of 10°N and a longitude of 180°E. The area is characterized by relatively smooth, dust-covered terrains (El Maarry et al. 2015).

The illumination history of this area is shown in Fig. 2 (right panel). The region is illuminated along the whole orbit, with a strong maximum of irradiance at the time of perihelion (2015 August).

Also for this location, in order to characterize the kind of activity typical of the area, plots are shown relative to a period of low activity (2014 January 19–23, when the comet was at a heliocentric distance of 4.55 au pre-perihelion) and to a period of high activity centred around the perihelion time (a heliocentric distance of 1.243 au).

During the low-activity period the area is illuminated for 3 hr per cometary day, and the maximum solar elevation angle is 72°. Similarly to what was happening at location A when it was found in a similar illumination regime, surface temperatures (Fig. 8) are comparable in both Cases, while internal temperatures are higher for Case 2, with a difference of 10 K at 2.5 cm. At a depth of 10 cm below the surface the temperature is stable at 75 K for Case 1, while for Case 2 the temperature is

still influenced by the solar input and is oscillating by a couple of degrees around 88 K. The gas flux, composed of CO_2, is

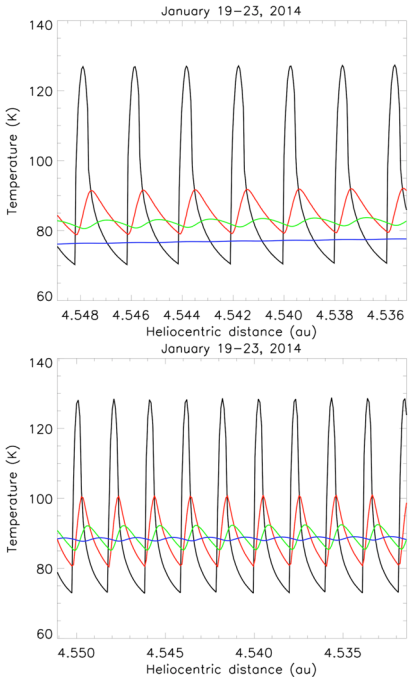

Figure 8. Case 1 (upper panel) and Case 2 (lower panel), location B, 2014 January 19–23: temperatures on the surface (black line) and in the layers below the surface (red line, 2.5 cm; green line, 5 cm; blue line, 10 cm).

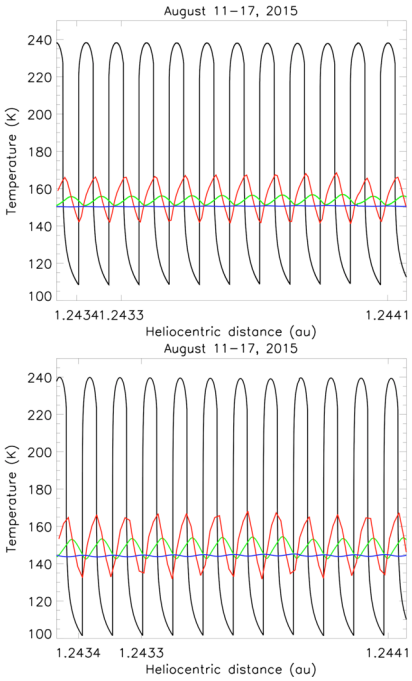

Figure 9. Case 1 (upper panel) and Case 2 (lower panel), location B, 2015 August 11–17: temperatures on the surface (black line) and in the layers below the surface (red line, 2.5 cm; green line, 5 cm; blue line, 10 cm).

very low for both Cases, and the dust flux is negligible. In the interior, nothing is changing and the depth of sublimation and the amorphous–crystalline transition fronts remain stable.

As for location A, at the time of perihelion the situation changes dramatically. Plots are shown for the period 2015 August 11–17; the area is illuminated for 6 hr per cometary day, and the minimum solar incidence angle is 26.°5.

The main difference between the two Cases is the nighttime temperature, which is lower for Case 2 than for Case 1, while the maximum surface temperature is 240 K. At a depth of 10 cm below the surface, the temperature remains constant at 150 K in Case 1, while it oscillates slightly around 145 K in Case 2 (Fig. 9).

In both cases, the water gas flux reaches a maximum of 1028 molec s^{-1} m^{-2} (Fig. 10); the CO_2 flux is slightly higher in Case 2. In both Cases, CO_2 sublimates from a layer at a constant temperature, as can be seen from the lack of difference between night and day. The dust flux reaches a maximum during the cometary day of 103 kg s^{-1} for Case 2, and is slightly lower for Case 1 (Fig. 11).

The stratigraphy of location B during most of its activity period is shown in Fig. 12. For Case 1, the amorphous–crystalline ice transition front, which was 2 cm under the surface before the beginning of the activity period, is, at its end, 1.1 m below the surface. The CO_2 sublimation front sinks, in the same period, by 50 cm, and the surface recedes by 15 cm.

Surface erosion is higher in Case 2 by 5 cm; at the end of the activity period the CO_2 sublimation front is less than 25 cm under the surface, and the amorphous ice transition front is 85 cm from the surface.

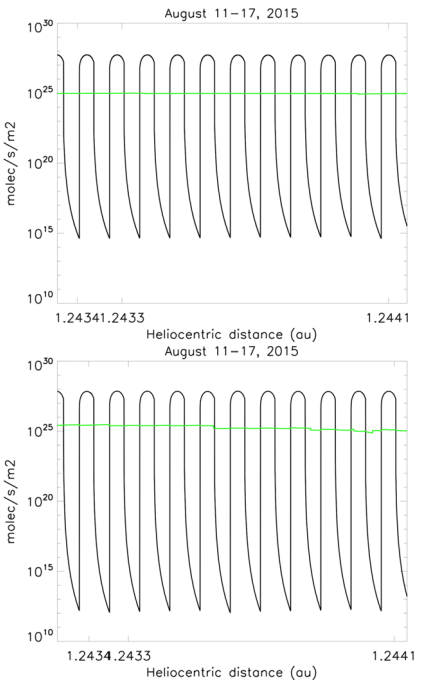

Figure 10. Case 1 (upper panel) and Case 2 (lower panel), location B, 2015 August 11–17: water flux (black line) and CO_2 flux (green line).

5 DIFFERENCES BETWEEN THE TWO LOCATIONS

In order to fully characterize the thermophysical behaviour in the two locations it is necessary to follow the activity along the orbit, taking into account the different illumination regimes, and to determine the erosion and the sinking of active fronts along the whole orbital period.

From Fig. 2 it can be seen that at perihelion in both locations irradiance reaches the same maximum value of 800 W m^{-2}, but for the remaining part of the orbit there are large differences. Location A even experiences a 6-week period of constant illumination, and

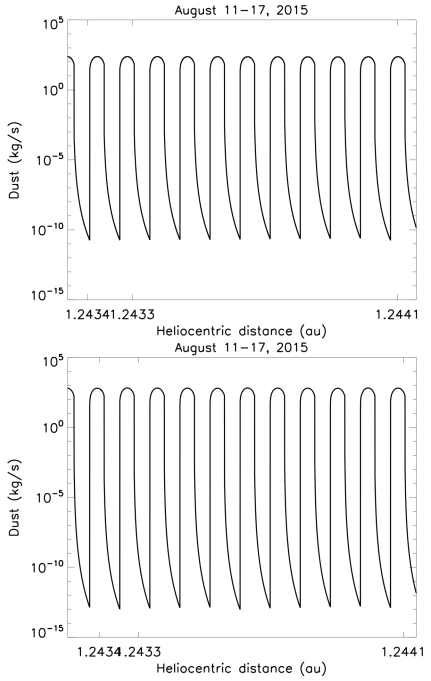

Figure 11. Case 1 (upper panel) and Case 2 (lower panel), location B, 2015 August 11–17: dust flux.

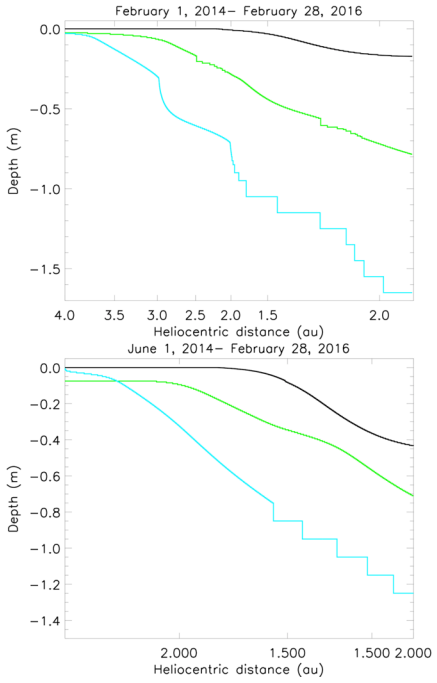

Figure 12. Case 1 (upper panel) and Case 2 (lower panel), location B, 2014 February 1 – 2016 February 28: stratigraphy showing the surface (black line), the CO_2 sublimation front (green line) and the amorphous ice transition front (blue line).

then the irradiance begins to decrease quickly, and already at 2 au postperihelion the values are lower than at location B (200 rather than 300 W m^{-2}). A long period of constant darkness follows. At location B the illumination conditions are much less extreme: after the perihelion passage the irradiance decreases but always has higher values than those at location A.

For both locations, the bulk of the activity tends to be concentrated around the time of perihelion, giving rise to a high erosion rate. The consequences of the different illumination regimes manifest themselves in the global behaviour of the two regions along the whole orbit. In the Anhur region, after the perihelion peak, the activity quickly decreases and then stops well in advance of the aphelion, when years of constant darkness begin. This clearly freezes the conditions that were created at the end of the time of perihelion. The activity restarts at 3 au preperihelion, when the area moves rapidly towards the intense activity peak of the perihelion, during which the surface tends to be rejuvenated more than other areas of the nucleus experiencing different illumination regimes. Remote sensing data acquired by *Rosetta* support the result that this area undergoes a stronger erosion during the perihelion time: see for example, the lack of dust-covered and smooth terrains (Fornasier et al. 2015). Location B never experiences a real freezing and its activity follows a more continuous trend, never ceasing completely, probably not even around the aphelion when ices more volatile than CO_2 could keep on sublimating.

6 DISCUSSION

A point that must be discussed is how adequate the model is to simulate and interpret the results obtained by *Rosetta*. The dust size distribution adopted in the modelling is truncated with respect to the largest particles seen in the coma, because larger particles cannot be lifted off through the process simulated in the numerical code. It is possible that more than a single process is at work and contributes to the dust ejection from the surface of the comet. The physical processes responsible for the frequent outbursts seen by the instruments onboard *Rosetta* (e.g. Feldman et al. 2016) could be different from the more 'gentle' processes at work for the rest of the time. Larger particles are lifted off more easily during an outburst. All of these processes contribute to the ablation of the surface, together with phenomena associated with the formation of cracks and areas of subsidence. The surface is further altered by the redeposition of the emitted dust, a widespread phenomenon especially in the northern regions (El Maarry et al. 2015).

The results of the modelling must be compared, when possible, with the thermal measurements retrieved by VIRTIS and MIRO. VIRTIS can sample the outermost surface layer, which is as thick as some tens of microns given the spectral range limited to $\leq 5.1\ \mu$m, the very low surface albedo and consequently the high thermal emissivity. To some extent, VIRTIS may sample surface temperatures between 150 and 170 K but with poor accuracy, so we have only diurnal temperatures for warm to hot areas, with a maximum value of 327 K achieved on 2015 August 9 (a few days prior to the perihelion passage, at a heliocentric distance of 1.44 au) at a latitude of 30.7° S and a longitude of 38.3° E. MIRO, however, does not suffer from this limitation in sensitivity and samples shallow subsurface temperatures on both the dayside and the nightside of the nucleus, down to depths depending on the specific channel being used and on the thermosphysical properties of the layer.

A direct comparison between theoretical temperatures obtained from our model and direct measurements obtained by both VIRTIS and MIRO is beyond the scope of this work, and is complicated by a number of reasons such as the lack of simultaneous coverage, substantially different spatial resolutions, different sensitivities and problems in the interpretation of the data. Because in the spectral range sampled by VIRTIS the temperature is a non-linear function of radiance, with a larger weight of the hottest subpixel features, the temperature obtained by VIRTIS is representative of the subpixel

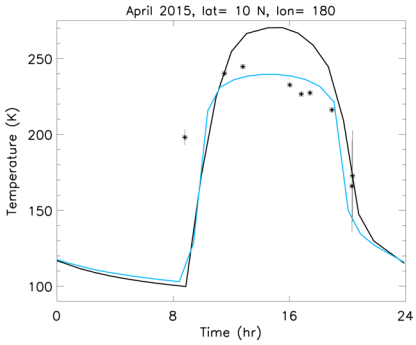

Figure 13. Location B, surface temperature on April 25 for Case 2 (blue line) and a Case in which the surface is completely dry (black line). The asterisks represent temperature values detected by VIRTIS during the month of 2015 April on a spot centred on location B.

regions at higher temperatures modulated by their effective areas, while a theoretical temperature can only represent a well-defined Case. In order to properly reproduce a measured temperature we would need to study the spot to which the temperature corresponds and combine the results of different theoretical curves.

The analysis of the temperatures detected by VIRTIS is still in progress and will be the subject of a separate work (Tosi et al., in preparation), but a first comparison with theoretical temperatures can be seen in Fig. 13. In the plot, daily theoretical temperatures representative of location B on April 25 are compared with VIRTIS measurements (shown as asterisks) taken during the month of April on a small spot centred on the same location. The black curve corresponds to a Case in which the surface is completely dry, while the blue curve corresponds to Case 2. The plot demonstrates that at the time of the VIRTIS measurements the spot was undergoing sublimation, but dry patches with much higher temperatures were contributing to the detected temperatures. So, we can conclude that theoretical temperatures can be used to reproduce measured temperatures.

The comparison between the measured gas and dust fluxes and the theoretical ones is even more complicated and will be the subject of a paper now in preparation. However, by taking advantage of model simulations (Fougère et al. 2016 a, b) it was possible to infer the water production rate from VIRTIS-M data, at about 1.88 au (Migliorini et al. 2016), and from VIRTIS-H data acquired close to perihelion Bockelée-Morvan et al. 2016). The estimated production rate is of the order of 4×10^{26} molec s^{-1} at 1.88 au (Fougère et al. 2016a), it increases to a value of 3×10^{27} molec s^{-1} at 1.5 au pre-perihelion, and finally reaches 1.5×10^{28} molec s^{-1} at perihelion (Fougère et al. 2016b). The CO_2 to H_2O ratio is fairly constant with the heliocentric distance, while quite a high value for the CO_2 production rate (8×10^{26} molec s^{-1} at perihelion and 9×10^{25} molec s^{-1} at 1.5 au pre-perihelion) is derived from the DSMC model applied to VIRTIS-H data (Fougere et al. 2016b). However, CO_2 reaches a maximum of $\sim 6 \times 10^{27}$ molec s^{-1} about 2 weeks after perihelion (Fougère et al. 2016b). It can be concluded that the results of the model compare reasonably well with the results of the observations.

More than 1 m of erosion has been estimated by Keller et al. (2015); when comparing this number with the values given in this paper it must be considered that the erosions reported in that paper are (porous) pure-ice equivalent erosions. The erosion estimated from our model can be considered as a lower limit, owing to the limitations in the code as far as the simulation of the ejection of dust grains is concerned. At present, the code cannot simulate the ejection of grains bigger than 10 cm, which are relatively common in the coma of the comet and contribute strongly to both dust flux and erosion.

6 CONCLUSION

The results of the model predict that, owing to the interplay between erosion and the sinking of the sublimation front, the thickness of the active layer should remain of the order of 1 m. This is consistent with the diurnal and orbital skin depth that can be inferred from the thermal inertia derived by MIRO and the instruments onboard *Philae*. We can conclude that the interior of the comet, below a layer of a few tens of centimetres, is pristine. This is also the minimum depth at which a future sample-return mission should probe, if aimed at taking really primitive, unprocessed material.

ACKNOWLEDGEMENTS

The authors would like to thank the following institutions and agencies that supported this work: the Italian Space Agency (ASI-Italy), the Centre National d'Etudes Spatiales (CNES-France), the Deutsches Zentrum für Luft und Raumfahrt (DLR Germany), and the National Aeronautic and Space Administration (NASA-USA) Rosetta Program, Science and Technology Facilities Council (UK).

Visible InfraRed Thermal Imaging Spectrometer (VIRTIS) was built by a consortium that includes Italy, France and Germany, under the scientific responsibility of the Istituto di Astrofisica e Planetologia Spaziali of Italian National Astrophysics Institute (INAF), Italy, which also guides the scientific operations. The VIRTIS instrument development is funded and managed by ASI, with contributions from the Observatoire de Meudon financed by CNES, and from DLR.

The authors wish to thank the Rosetta Science Ground Segment and the Rosetta Mission Operations Centre for their dedication and support throughout the phases of the mission.

REFERENCES

Acton C., 1996, Planet. Space Sci., 44, 65
Auger A.-T. et al., 2015, A&A, 583, 35
Balsiger H. et al., 2007, Space Sci. Rev., 128, 745
Bar-Nun A., Laufer D., 2013, Planet. Space Sci., 86, 160B
Barucci et al., 2016, A&A, 595, 102
Bertaux J.-L. et al., 2015, A&A, 583, 38
Blum J. et al., 2014, Icarus, 235, 156B
Bockelée-Morvan D., Crovisier J., Mumma M. J., Weaver H. A., 2004, in Festou M.C., Keller H.U., Weaver H., eds, Comets II. University of Arizona Press, Tucson, p. 391
Bockelée-Morvan et al., 2016, MNRAS, 462, S170
Capaccioni F. et al., 2015, Science, 347, 628
Capria M. T. et al., 2009, A&A, 504, 249
Capria M. T. et al., 2012, A&A, 537, 71
Choukroun M. et al., 2015, A&A, 583, 28
Colangeli L. et al., 2007, Space Sci. Rev., 128, 803
Collings M. P. et al., 2004, MNRAS, 354, 1133
Coradini A. et al., 2007, Space Sci. Rev., 128
De Sanctis M. C., Capria M. T., Coradini A., 2006, Adv. Space Res., 38, 1906
De Sanctis M. C., Lasue J., Capria M. T., 2010, AJ, 140, 1
De Sanctis M. C. et al., 2010, Icarus, 307, 241
De Sanctis M. C. et al. 2015, Nature, 525, 500
El-Maarry M. R. et al., 2015, A&A, 583, 26
Feldman P. et al., 2016, ApJ, 825 L8
Filacchione G. et al., 2015, Nature, 529, 368
Filacchione G. et al., 2016, Science, 354, 1563

Fornasier S. et al., 2015, A&A, 583, 30
Fornasier S. et al., 2016, Science, 354, 1566
Fougere N. et al., 2016a, A&A, 588, 134
Fougere N. et al., 2016b, MNRAS, 462, 156
Fulle M. et al., 2015, ApJ, 802, L12
Fulle M. et al., 2016, ApJ, 821, L19
Fuselier S. A. et al., 2015, A&A, 583, 2
Gulkis S. et al., 2007, Space Sci. Rev., 128, 561
Gulkis S. et al., 2015, Science, 347, 709
Gundlach B., Blum J., 2012, Icarus, 219, 618
Johansen A. et al., 2007, Nature, 448, 1022
Jorda L. et al., 2016, Icarus, 277, 257
Keller H. U. et al., 2007, Space Sci. Rev., 128, 433
Keller H. U. et al., 2015, A&A, 583, 34
Kofman W. et al., 2007, Space Sci. Rev., 128, 413
Kofman W. et al., 2015, Science, 349, 639
Le Roy L. et al., 2015, A&A, 583, 1
Lee S. et al., 2015, A&A 583, A5
Lee J. et al., 2016, MNRAS 462, S573
Lucchetti A. et al., 2016, A&A, 585, L1
Mall U. et al., 2016, ApJ, 819, 126
Maquet L., 2015, A&A, 579, 78
Migliorini A. et al., 2016, A&A, 589, 45
Mottola S. et al., 2014, A&A, 569, L2
Mumma M. J., Charnley S. B., 2011, ARA&A., 49, 471
Pätzold M. et al., 2016, Nature, 530, 63
Pfalzner S. et al., 2015, Phys. Scr., 90, 068001
Pommerol A. et al., 2015, A&A, 583, 25
Raponi A. et al., 2016, MNRAS, 462, S476
Rotundi A. et al., 2015, Science, 347, 3905
Rubin M. et al., 2015, Science, 348, 232
Schloerb F. P. et al., 2015, A&A, 583, 29
Schulz R., 2012, Planet. Space Sci., 66, 1
Sierks H. et al., 2015, Science, 347, 1044
Skorov Y., Blum J., 2012, Icarus, 221, 1
Spohn T. et al., 2007, Space Sci. Rev., 128, 339
Spohn T. et al., 2015, Science, 349, 464
Thomas N. et al., 2015, Science, 347, 6220
Tosi F. et al., 2015, Geophysical research Abstracts, 17, EGU2015-11625
Vincent J.-B. et al., 2015, Nature, 523, 63

This paper has been typeset from a Microsoft Word file prepared by the author.